Prabha Materials Science Letters
Vol. 5, No. 2, 403-411, 2026
https://doi.org/10.33889/PMSL.2026.5.2.022

Optimization of Doping Concentration for Upconversion Emission from $Zn_2GeO_4:Er^{3+}$ Phosphor

Anurag Pandey
Department of Physics,
University of the Free State, P. O. Box 339, Bloemfontein 9300, South Africa.
&
Ballipur, Banewara, Mariyahu, Jaunpur, Uttar Pradesh, 222128, India.
E-mail: anuragpandey439@gmail.com

Sumit Kumar
Department of Chemistry,
Bharat Sevak Samaj College, Supaul, B. N. Mandal University, Madhepura, Bihar, India.
E-mail: sumitdhn@gmail.com

Promod Kumar
Laboratoire Hubert Curien,
UMR 5516, Universit´e Jean Monnet Saint-Étienne, CNRS, 42023, Saint-Etienne, France
E-mail: promod.kumar@univ-st-etienne.fr, pkpmcm@gmail.com, talk2promodthakur@gmail.com

R. E. Kroon
Department of Physics,
University of the Free State, P. O. Box 339, Bloemfontein 9300, South Africa.
E-mail: KroonRE@ufs.ac.za

Vinod Kumar
Department of Physics,
The University of the West Indies, St. Augustine, Trinidad and Tobago.
Corresponding author: vinod.phy@gmail.com, vinod.kumar@uwi.edu

H. C. Swart
Department of Physics,
University of the Free State, P. O. Box 339, Bloemfontein 9300, South Africa.
E-mail: swarthc@ufs.ac.za

(Received on November 13, 2025; Revised on February 10, 2026 & June 17, 2026 & June 29, 2026; Accepted on July 2, 2026)

Abstract
The upconversion (UC) emission behavior of Er^{3+}-activated Zn_2GeO_4 phosphors synthesized using a solid-state reaction technique was reported. A series of phosphors was prepared by varying the dopant concentration to optimize the emission for optical purposes. The phase formation of the Zn_2GeO_4 was confirmed through X-ray powder diffraction analysis, and a negligible effect of the dopant on the structure was found. Scanning electron microscopy analysis was performed to examine the grain size and its formation. It was found that micro-sized, well-arranged grains were present throughout the phosphor. The influence of doping concentration on the UC emission spectra has been recorded by using 980 nm excitation. The comparison of UC emissions shows 2 mol% of Er^{3+} is the optimum doping concentration in the present host to achieve maximum upconversion emission. A schematic energy level structure is proposed to display the observed upconversion emission of the $Zn_2GeO_4:Er^{3+}$ phosphor.

Keywords- Upconversion, Zn_2GeO_4, Erbium ions, Concentration dependence, Two photon processes.

1. Introduction

Rare-earth (RE) doped luminescent materials have widespread applications that depend on the spectral emission observed (Pandey and Rai, 2014; Zhou et al., 2015; Pandey et al., 2018). Luminescence detected from these materials is primarily controlled by the rare-earth centers of the dopant and the crystal fields of the host matrix. Therefore, the selection of doping rare-earth ions and a corresponding suitable host reflects efficient optical emissions. Among rare-earths, erbium is widely used as a doping element, especially for its emission in the triply ionized state, Er^{3+}, which exhibits prominent emission transitions, such as the $^2H_{11/2} \rightarrow {}^4I_{15/2}$ and $^4S_{3/2} \rightarrow {}^4I_{15/2}$ transitions (Wang et al., 2012). To achieve maximum optical emission intensity from the doped material, one should first optimize its concentration and then adjust other parameters. The multimodal emission and excitation capacity of Er^{3+} throughout the visible and near-infrared range, along with other physical-chemical properties, greatly attracts researchers (Verma et al., 2011).

Upconversion (UC) emission detected from various lanthanides activated phosphor materials having wide range from UV-Vis to NIR region. These light emissions in different regions display their utilization in different technological fields. For example, NIR lights have applications in biomedical field like bioimaging, cellular labeling, deep tissue and animal imaging, drug delivery and bio-sensing (Eraky et al., 2025; Zhang et al., 2025). Solar spectrum conversion, security ink, 3D printing, temperature sensing and environmental monitoring like applications show more utilization of UV-Vis light emissions from UC materials (Shah et al., 2022; Pandey et al., 2023). Polymerically engineered UC nanoparticles have also attracted researchers as agents for functionally modified coherent tomography (Mohan and Poddar, 2021).

Numerous compounds have been used as host materials with embedded rare-earth ions in them for structural and optical investigations, but oxide hosts are the center of attraction. Zinc germinate (Zn_2GeO_4) has also been recently used as an oxide host material, due to its wide band gap, high photon response, and other features (Gao et al., 2017). Previously, various rare-earth and transition-metal-embedded Zn_2GeO_4 phosphors have been studied for different applications (Gao et al., 2017; Hu et al., 2017; Chen et al., 2024). Gao et al. (2017) prepared Tb^{3+} doped Zn_2GeO_4 nanophosphors and observed green/blue light emission upon 265 nm ultraviolet (UV) excitation. Hu et al. (2017) observed a green emission band upon 322 nm excitation in a Mn^{2+}-doped Zn_2GeO_4 material synthesized by a high-temperature solid-state route. Er^{3+} is a well-known laser-active ion with abundant energy levels and notable emission characteristics, which is making it suitable for numerous applications (Gálico et al., 2024; Qiao et al., 2025). Recently, Chen et al. (2024) have investigated Er^{3+}-Yb^{3+} codoped Zn_2GeO_4 phosphors and studied their optical properties at different excitations. However, the doping concentration was not optimized.

In the present study the effect of doping concentration on structural, morphological and optical properties of Zn_2GeO_4:Er^{3+} phosphor was investigated. The UC emission study of Zn_2GeO_4:Er^{3+} phosphor upon a 980 nm excitation via varying concentrations of Er^{3+} ions were reported. To understand the UC mechanism in Zn_2GeO_4:Er^{3+} phosphor, a schematic diagram was also presented.

2. Experimental Details

2.1 Material Preparation

The Zn_2GeO_4:Er^{3+} phosphors were synthesized by the high-temperature solid-state reaction method (Hu et al., 2017). A mixture containing analytical grade GeO_2, ZnO, and Er_2O_3 in an appropriate ratio (at varying concentrations of erbium: 0 mol%, 0.1 mol%, 0.5 mol%, 1 mol%, 2 mol%, 3 mol%, and 5 mol%) were mixed in a mortar and ground for about 2 h using acetone as a mixing medium. The fine mixture powders were placed into alumina crucibles and preheated at 800°C for 6 h in a furnace, followed by further heat

treatment at 1300°C for 6 h in air. Finally, the formed samples were well ground into fine powder and further used for structural, morphological and optical studies.

2.2 Characterization

The X-ray powder diffraction (XRPD) measurement was performed by using Bruker D8 focus diffractometer with Cu target radiation (λ = 0.154056 nm) to identify phase formation and crystallite size of the prepared phosphors. The scanning electron microscopy (SEM) and energy-dispersive X-ray spectroscopy (EDS) images were obtained using a JSM-7800F extreme-resolution analytical field-emission scanning electron microscope. The vibrational stretching modes of the undoped and Er^{3+} doped Zn_2GeO_4 phosphors were further studied using a Fourier transformed infra-red (FTIR) Perkin Elmer spectrometer in the transmission mode. The UC emission spectra of the developed phosphors were recorded using a Horiba iHR-320 monochromator upon a 980 nm diode laser excitation with limit up to 3 W.

3. Results and Discussions

3.1 Structural and Morphological Analysis

Figure 1 shows the X-ray powder diffraction patterns of undoped and Er^{3+} doped Zn_2GeO_4 phosphors in the range of 10 to 80°. Well-observed, sharp diffraction peaks of good intensity indicated the high crystallinity of the prepared undoped and Er^{3+} doped Zn_2GeO_4 phosphors materials. All the diffraction peaks were assigned perfectly with those of the standard pattern (JCPDS No.: 11-0687) of rhombohedral structured Zn_2GeO_4 with R3 space group (Hu et al., 2017). All the strong diffraction peaks were index with their miller indices. Most prominent peak around 2θ = 33˚ corresponding to the (410) plane. Main diffraction peaks were observed between 30° and 35° in all cases, with slight variations in peak intensities. Other diffraction peaks maintain almost identical positions in both undoped and Er^{3+}-doped Zn_2GeO_4 phosphors. The peak around 12° exhibited a slight shift towards a lower 2θ value and a slight random change in peak intensities. These changes may be due to differences in the ionic radii of Zn^{2+} and Er^{3+} ions (Gao et al., 2017). Overall, no significant influence was observed on the incorporation of the doping element, which resulted in the Zn_2GeO_4 structure.

The crystallite size of undoped and Er^{3+} doped Zn_2GeO_4 phosphors was calculated by the Debye-Scherrer formula (Kumar et al., 2022).

$$D = \frac{K\lambda}{\beta\, Cos\theta}.$$

where, D is the representing crystallites size of undoped and Er^{3+} doped Zn_2GeO_4, λ is the wavelength of Cuk_α radiation (1.541 Å), K is the correlation factor, β is presented by the Full width at half maximum (FWHM) of the diffraction peak and θ is the Bragg's diffraction angle. The crystallite size of the Zn_2GeO_4 was varying from 33 to 53 nm with variation in the doping concentration.

The surface morphology of the Er^{3+}-doped Zn_2GeO_4 phosphor was studied via a SEM image given in **Figure 2(a)**. The image scale bar is 1 µm, and the image displays a well-arranged distribution of grains throughout the surface. The sizes of the grains were estimated to be between 0.5 and 2.5 µm, resulting in the formation of micro-sized grains in the prepared Er^{3+}-doped Zn_2GeO_4 phosphors.

Figure 2(b) shows the EDS spectrum of the Er^{3+}-doped Zn_2GeO_4 phosphor material to confirm the presence of elemental composition. Clearly, the spectrum reflects that Zn, Ge, O, and Er were all present in proper weight percentage. Therefore, we found that the present material, prepared by the high-temperature solid-state route, exhibits a good surface morphology.

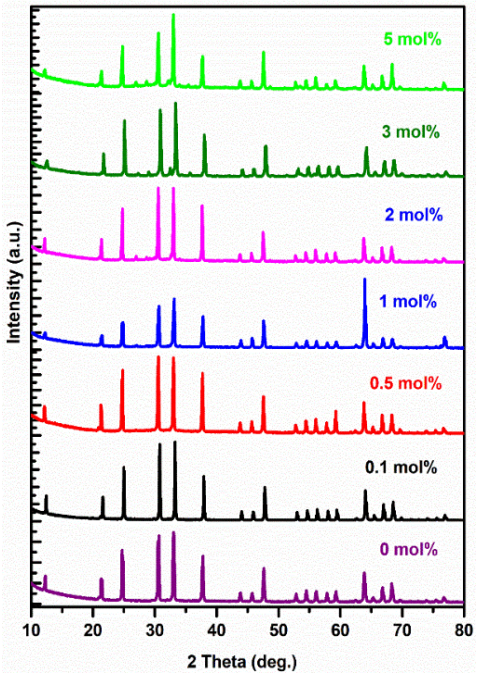

Figure 1. Effect of doping concentration on the XRD pattern of Zn_2GeO_4 phosphors.

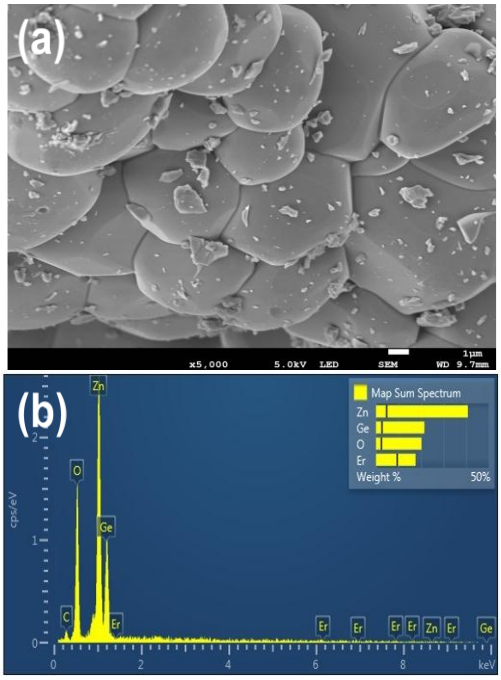

Figure 2. (a) SEM image, and (b) EDS image of the 2 mol % Er^{3+}-doped Zn_2GeO_4 phosphor.

The elemental compositions of the Zn_2GeO_4 are examined using EDS analysis is shown in **Figure 3**. The results of EDS elemental mapping confirmed the presence of Zn, O and Ge elements in the Zn_2GeO_4 host matrix. The maps show that the elements are well distributed throughout the analyzed region, indicating good compositional uniformity. No significant elemental segregation or agglomeration was observed, suggesting the successful formation of the material.

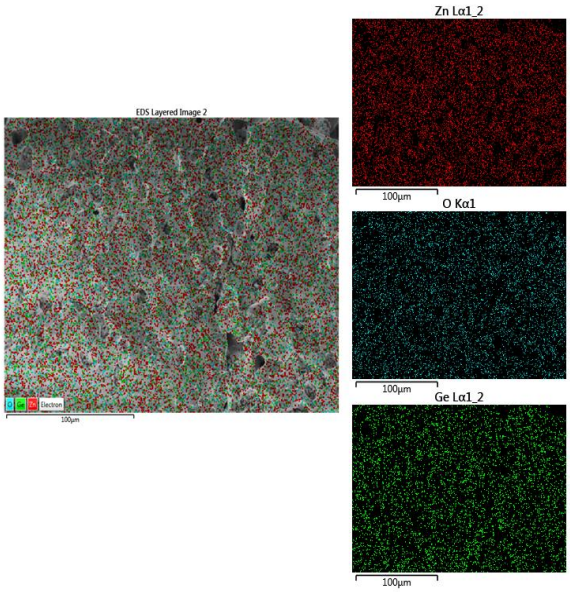

Figure 3. EDS spectra with elemental mapping for Zn_2GeO_4.

3.2 FTIR Analysis of Undoped and Er^{3+} Doped Zn_2GeO_4 Phosphors

The FTIR spectra of undoped and Er^{3+} doped Zn_2GeO_4 phosphors, recorded over the spectral range 600–3000 cm^{-1}, are depicted in **Figure 4**. A pronounced absorption band centered at approximately 734 cm^{-1} corresponds to the stretching vibrations of Ge–O bonds within the (GeO_4) tetrahedral units or the Zn–O–Ge linkages inherent to the rhombohedral Zn_2GeO_4 structure. This mode is recognized as the signature vibrational fingerprint of the Zn_2GeO_4 crystalline phase, thereby confirming the establishment of the host lattice framework (Wu and Ma, 2013, Calderón-Olvera et al., 2023). In the Er^{3+}doped sample, a comparable absorption band near 734 cm^{-1} is also observed, indicating that Er^{3+} ion incorporation does not significantly perturb the primary crystal lattice. Nevertheless, a marginal increase in band intensity and broadening is evident, which can be attributed to local structural distortions induced by substitutional doping of Er^{3+} ions into the Zn_2GeO_4 matrix. Additionally, a weak absorption feature near 2364 cm^{-1} is detected exclusively in the doped specimen. This band is ascribed to the asymmetric stretching vibration of atmospheric CO_2 adsorbed on the sample surface during spectral acquisition, consistent with literature reports where similar CO_2-related bands manifest in the 2330–2360 cm^{-1} region for oxide materials (Dolson and Anders, 2015).

The absence of discernible absorption bands related to residual organic species or synthesis by-products indicates efficient decomposition during processing and the formation of a high-purity phase. Overall, the spectral congruence between the undoped and Er^{3+} doped Zn_2GeO_4 samples demonstrates that Er^{3+} doping proceeds without inducing detectable secondary phases or fundamental alterations in the host lattice, as evidenced by FTIR analysis.

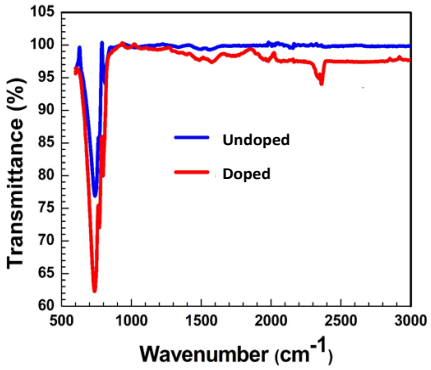

Figure 4. FTIR spectra of undoped and Er^{3+} doped Zn_2GeO_4 phosphors.

3.3 UC Emission Study

The room temperature UC emission spectra of the Zn_2GeO_4:Er^{3+} phosphor in the 400-850 nm wavelength range upon excitation with a 980 nm diode laser is shown in **Figure 5** with increasing the doping concentration from 0.1 to 5 mol%. Three prominent UC emission bands were found, namely green (515 to 575 nm), red (640 to 690 nm) and NIR (780 to 850 nm) regions. These emission peaks are assigned suitably for various transitions of Er^{3+} ion. The green emission band is assigned through $^2H_{11/2}\rightarrow{}^4I_{15/2}$ and $^4S_{3/2}\rightarrow{}^4I_{15/2}$ transitions, the red band through $^4F_{9/2}\rightarrow{}^4I_{15/2}$ transition, and the NIR band through $^4I_{9/2}\rightarrow{}^4I_{15/2}$ transition of the erbium ion (Dieke, 1968; Nair et al., 2023; Tu et al., 2024; Qiao et al., 2025).

No UC emission was observed in the case of undoped Zn_2GeO_4 phosphor, so it is not included in **Figure 5**. Emission spectra of phosphors at 0.1 mol%, 0.5 mol%, 1 mol%, 2 mol%, 3 mol%, and 5 mol% of Er^{3+} doped Zn_2GeO_4 are plotted on the same scale together to find the optimized concentration. On comparing emission spectra, the following observations were noted:

(1) Green UC emission band has a maximum intensity for 3 mol% of Er^{3+} doping.
(2) Red UC emission band has a maximum intensity for 2 mol% of Er^{3+} doping.
(3) For lower doping levels, samples initially exhibited red light emission from 0.1 mol% to 2 mol% Er^{3+} doping and then shifted to green light emission from 3 mol% to 5 mol% Er^{3+} doping. This abrupt change in UC emission intensity on increasing dopant concentration shows the color-tuning ability of the present phosphor material. When we compared the integrated intensity of both green and red bands at 2 mol% and 3 mol%, respectively, it results in 2 mol% of Er^{3+} doping being the optimum.

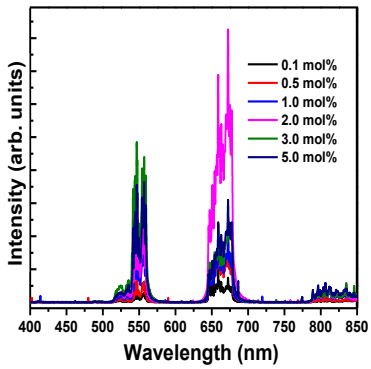

Figure 5. UC emission spectra of the Er^{3+} doped Zn_2GeO_4 phosphors with different doping concentration upon 980 nm excitation.

To understand the number of photons in the UC process, a power dependence study of UC emission was performed, and it was found that two UC photons are involved in both green and red emissions. A transition mechanism involved in the present investigation through ground state absorption (GSA) and excited state absorption (ESA) processes is shown in **Figure 6**.

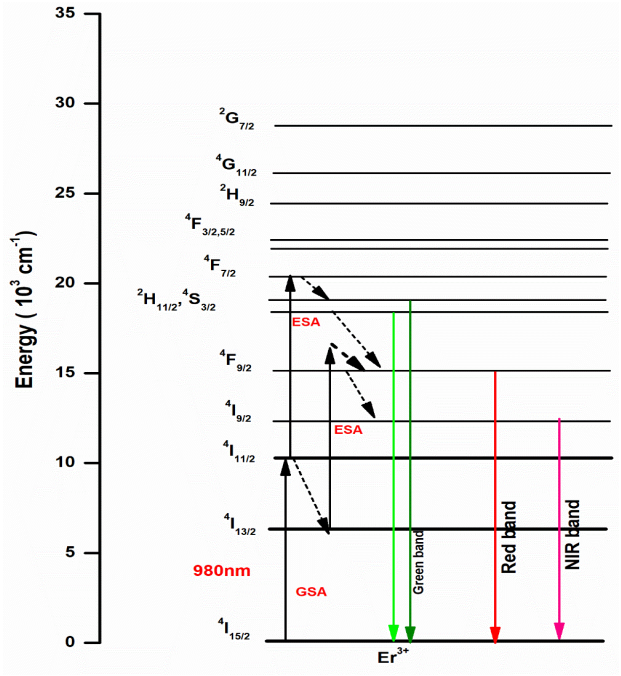

Figure 6. Energy level diagram of the Er^{3+} ion for doped Zn_2GeO_4:Er^{3+} phosphor.

The proposed energy scheme for the Er^{3+} ion indicates that the $^4I_{11/2}$ state is populated through the ground state absorption (GSA) process. As in our case, two different colors of light are emitted at 2 mol% and 3 mol% emissions; therefore, we have two excited-state absorption pathways. The $^2H_{11/2}$, $^4S_{3/2}$ levels are populated by sequential absorption of 980 nm pump photons through GSA and ESA processes and relax to ground level $^4I_{15/2}$ by dominant green emission (as in the case of 3 mol% doping). The $^4F_{9/2}$ level is populated by the GSA and ESA process through non-radiative relaxation from $^4I_{11/2}$ to $^4I_{13/2}$. Radiative relaxations from the $^4F_{9/2}$ to $^4I_{15/2}$ level exert dominant red emission (as in the case of 2 mol% doping). Weak NIR emission was also detected from the $^4I_{9/2}$ to $^4I_{15/2}$ transition, which is populated by non-radiative relaxation from $^4F_{9/2}$ to $^4I_{9/2}$ levels.

4. Conclusions

The successful synthesis of the undoped and Er^{3+}-doped Zn_2GeO_4 phosphors through a solid-state reaction was verified. The structural study showed that the phase of phosphors remained unchanged when the doping concentration of Er^{3+} was varied. The presence of each element was verified in the micro-sized grains distributed throughout the surface. Two-photon pumped UC emission spectra of the Zn_2GeO_4:Er^{3+} phosphors were compared as the Er^{3+} concentration changed, resulting in optimum red emission at 2 mol% and green emission at 3 mol%. This change in the color of light emitted from the present phosphor is proposed due to a change in the population of the excited states when the Er^{3+} concentration was changed from 2 mol% to 3 mol%. Overall, the 2 mol% Er^{3+} concentration is best for achieving maximum emission intensity.

Conflicts of Interest
The authors declare no conflict of interest.

Acknowledgments
This research is supported by the South African Research Chairs Initiative of the Department of Science and Technology (84415) and the University of the Free State, Bloemfontein.

AI Disclosure
The author(s) declare that no assistance is taken from generative AI to write this article.

References

Calderón-Olvera, R.M., Arroyo, E., Jankelow, A.M., Bashir, R., Valera, E., Ocaña, M., & Becerro, A.I. (2023). Persistent luminescence Zn2GeO4: Mn2+ nanoparticles functionalized with polyacrylic acid: one-pot synthesis and biosensing applications. *ACS Applied Materials & Interfaces*, *15*(17), 20613-20624. https://doi.org/10.1021/acsami.2c21735

Chen, X., Sha, X., Zhang, Y., Gao, D., Wang, L., Zhang, Y., Liu, T., Zhang, X., Zhang, J., Cao, Y., Wang, Y., Li, X., Xu, S., Yu, H., & Chen, B. (2024). Multicolor-emitting Er3+ and Er3+/Yb3+ doped Zn2GeO4 phosphors combining static and dynamic identifications for advanced anti-counterfeiting application. *Spectrochimica Acta Part A: Molecular and Biomolecular Spectroscopy*, *309*, 123830. https://doi.org/10.1016/j.saa.2023.123830.

Dieke, G.H. (1968). *Spectra and energy levels of rare earth ions in crystals.* Interscience Publishers, USA. ISBN 470 21390 6.

Dolson, D.A., & Anders, C.B. (2015). FTIR vibration-rotation spectrum and analysis of the 13CO2 asymmetric stretch fundamental band. *The Chemical Educator*, *20*(1), 53-59. https://doi.org/10.1333/s00897152601a

Eraky, M.S., Elsherif, S.S., & Sanad, M.M. (2025). recent trends in upconversion luminescent inorganic materials and nanomaterials for enhanced photovoltaic solar cell and biological applications. *Journal of Fluorescence*, *35*, 9205-9229. https://doi.org/10.1007/s10895-025-04198-x

Gálico, D.A., Rodrigues, E.M., Halimi, I., Toivola, J., Zhao, H., Xu, J., Moilanen, J.O., Liu, X., Hemmer, E., & Murugesu, M. (2024). Confining single Er3+ ions in sub-3 nm NaYF4 nanoparticles to induce slow relaxation of the magnetisation. *Nature Communications*, *15*(1), 3498. https://doi.org/10.1038/s41467-024-47682-x

Gao, X., Li, C., Li, S., Zhang, H., Li, Z., Hong, Y., Sun, J. (2017). Intense green/blue light emission of Zn_2GeO_4 nanophosphors doped Tb^{3+} ions under 265-nm excitation. *Journal of Luminescence 190*, 457-461. http://dx.doi.org/10.1016/j.jlumin.2017.05.075.

Hu, J.Q., Song, E.H., Ye, S., Zhou, B., & Zhang, Q.Y. (2017). Anomalous spontaneous-reduction of Mn 7+/Mn 4+ to Mn 2+ and luminescence properties in Zn 2 GeO 4: Mn. *Journal of Materials Chemistry C*, *5*(13), 3343-3351. https://doi.org/10.1039/c6tc05359a

Kumar, V., Tiwari, S.P., Etefa, H.F., Jule, L.T., Ntwaeaborwa, O.M., & Swart, H.C. (2022). Energy transfer mechanism in Eu3+ doped tin oxide nanophosphors for red solid state lighting. *Journal of Luminescence*, *250*, 119085. https://doi.org/10.1016/j.jlumin.2022.119085

Mohan, M., & Poddar, R. (2021). Polymerically engineered upconversion nanoparticles (UCNPs) as contrast agent for functionally modified optical coherence tomography (OCT). *Materials Science and Engineering: C*, *121*, 111841. http://dx.doi.org/10.1016/j.msec.2020.111841

Nair, G.B., Tamboli, S., Dhoble, S.J., & Swart, H.C. (2023). LaOF: Yb3+, Er3+ upconversion nanophosphors operating at low laser powers for nanothermometry applications. *ACS Applied Nano Materials*, *6*(16), 15255-15265. https://doi.org/10.1021/acsanm.3c03208

Pandey, A., Kumar, S., Kumar, V., & Swart, H.C. (2023). Comparative upconversion emission study of XWO4: Ho3+-Yb3+(X= Ba, Ca, Sr) phosphors. *Prabha Materials Science Letters*, *2*(1), 41-47. https://doi.org/10.33889/PMSL.2023.2.1.0034.

Pandey, A., Rai, V.K. (2014). Rare earth doped materials for temperature sensors. In: Dwivedi, Y., Rai, S.B., & Singh, J.P. (eds) *Spectroscopic Techniques for Security Forensic and Environmental Applications*, Nova publisher. USA, pp. 279-292.

Pandey, A., Tiwari, S.P., Dutta, V., & Kumar, V. (2018). Photon up conversion in lanthanide-activated inorganic luminescent materials. In: Tiwari, R., Dubey, V., & Dhoble, S.J. (eds) *Emerging Synthesis Techniques for Luminescent Materials*, IGI Global, USA, pp. 86-116.

Qiao, X., Liu, Y., Yang, X., & Tsuboi, T. (2025). Structural, luminescence and upconversion properties in Er doped LiYb (MoO4) 2 solid solution. *Ceramics International*, *51*(6), 6926-6936. https://doi.org/10.1016/j.ceramint.2024.12.127.

Shah, S.A.A., Sayyad, M.H., Sun, J., & Guo, Z. (2022). Recent advances and emerging trends of rare-earth-ion doped spectral conversion nanomaterials in perovskite solar cells. *Journal of Rare Earths*, *40*(11), 1651-1667. https://doi.org/10.1016/j.jre.2021.12.001

Tu, L., Wu, K., Luo, Y., Wang, E., Yuan, J., Zuo, J., Zhou, D., Li, B., Zhou, J., Jin, D., & Zhang, H. (2023). Significant enhancement of the upconversion emission in highly Er3+-doped nanoparticles at cryogenic temperatures. *Angewandte Chemie International Edition*, *62*(7), e202217100. https://doi.org/10.1002/anie.202217100

Verma, R.K., Kumar, K., & Rai, S.B. (2011). Dual mode emission and harmonic generation in ZnO–CaO–Al2O3: Er3+ nano-composite. *Journal of Luminescence*, *131*(5), 988-993. https://doi.org/10.1016/j.jlumin.2011.01.009

Wang, N., Zhang, X., Jiang, H., Dong, T., & Yang, D. (2012). Fabrication of Er3+/Yb3+ co-doped Y2O3 transparent ceramics by solid-state reaction method and its up-conversion luminescence. *Materials Chemistry and Physics*, *135*(2-3), 709-713. https://doi.org/10.1016/j.matchemphys.2012.05.048

Wu, S., & Ma, Q. (2013). Synthesis, characterization and microwave dielectric properties of Zn2GeO4 ceramics. *Journal of Alloys and Compounds*, *567*, 40-46. https://doi.org/10.1016/j.jallcom.2013.03.052

Zhang, J., Du, J., Jia, S., Li, Y., Ågren, H., Prasad, P.N., & Chen, G. (2025). Recent advances in upconversion nanoparticles for therapeutics: from fundamentals to cutting‐edge applications. *Electron*, *3*(3), e70012. https://doi.org/10.1002/elt2.70012

Zhou, J., Liu, Q., Feng, W., Sun, Y., & Li, F. (2015). Upconversion luminescent materials: advances and applications. *Chemical Reviews*, *115*(1), 395-465.